2023 IEEE International Conference on Robotics and Automation (ICRA 2023)
May 29 - June 2, 2023. London, UK

Computational Modeling in System with Non-Circular Timing Pulleys

Renzo Caballero†, Angelica Coronado†, and Eric Feron†

***Abstract*— We analyze and model a belt transmission system with non-circular timing pulleys. Using a 3D printer as a proof-of-concept device, experiments consisting of tracking the pose data of a printer nozzle and its pulleys are conducted. A computational model from our previous work is validated with the experimental data and expanded to model more complex systems with multiple non-circular timing pulleys as well as slippage and non-ideal tensions. Finally, an example with two non-circular timing pulleys is presented and simulated utilizing the proposed method.**

I. Introduction

Timing belt transmission systems are widely used in industrial robots and systems that require accurate power and motion transmission. Timing belt drives, which are of great importance for many fields, have many advantages such as small weight, low noise, high power transmission, high velocity, and high efficiency [1], [2]. However, they have a tendency to wear out due to intrinsic and external factors, affecting the reliability of the system [3]. Thus, a number of studies have investigated the diagnosis and detection of failures on timing belt drives [3]–[6]. These failures can occur due to the wear of their components [7], including timing pulleys [8] that can cause slippage and reduction of the precision of the system.

Although traditional ideal timing pulleys are circular, the literature describes systems that use non-circular pulleys for a range of applications. Some of the assumptions that are generally made for circular pulleys need to be re-considered for non-circular pulleys [9]. For instance, the use of non-circular pulleys might lead to a lack of proper belt tension due to the geometry of the pulley itself. In [10], methods are proposed in which elastic idlers are added to maintain the timing belt tension. Research efforts in the study of systems with non-circular pulleys include fabrication [11], weight compensation mechanisms [4], [12], [13], robotic joints [10], [14], and modeling of timing belt drives with non-circular pulleys [9].

To build upon our previous work [15], in which we constructed a computational model—and a formal mathematical model in [16]—to analyze the effect of a non-circular timing pulley on the x-axis of a 3D printer, here, we conduct a high-precision experiment to have a finer validation of the computational model in [15], and we generalize our model to a system with multiple non-circular timing pulleys. Our main contributions are (i) to validate with experimental data and consider teeth misalignment on the model proposed in [15], (ii) to provide a mathematical model for non-ideal tensions and slippage on the timing belt, and (iii) to combine both, the mathematical model from (ii) and the computational model proposed in [15], to simulate systems with multiple non-circular timing pulleys.

We conduct a set of experiments to capture 6 degrees-of-freedom (6-DoF) data from a belt drive system of a 3D printer when the printer x-axis motor has a non-ideal timing pulley. Traditional methods used to track the motion of 3D printer components include encoders, optical sensors, and motion capture systems [17], [18]. The experiments in this paper are performed using the motion capture system Optitrack, a real-time tracking system that offers high precision (0.01 mm), low system latency, and high resolution due to its data collection frequency of up to 360 frames per second. This tracking system is widely used for different applications; capturing face and body data [19], [20], tracking the position of drones [21], [22], robots [23]–[25], and mobile 3D printers [25]–[27] are among the most popular.

The paper is organized as follows: Section II contains the details of the performed experiment. Section III has the observations of the experimental data. Section IV describes the proposed models. Section V presents the validation and simulation of the proposed models. Section VI presents the closing conclusion.

II. Experiment Description

A. Goal of the Experiment and Notation

In this experiment, we aim to measure empirically the relationship between the rotation on the x-axis timing pulley—for any shape the timing pulley might have, circular or non-circular—, and the x-axis displacement of the printing nozzle. As we detailed in [15], for an ideal system with a circular x-axis timing pulley with radius r, when the pulley experiences an angular rotation $\Delta\theta$, the nozzle experiences a change of position Δx in the x-axis direction of magnitude $\Delta x = \Delta x(\Delta\theta) = \Delta\theta r$—see Fig. 1—. In such case, for infinitesimal rotations, the limit

$$\lim_{\Delta\theta\to 0} \frac{\Delta x(\Delta\theta)}{\Delta\theta} = r \tag{1}$$

is well-defined and independent of the angular position of the timing pulley.

An ideal pulley is defined as a circular pulley of the ideal radius r given by the design specifications, and it is the pulley

†Renzo Caballero (Renzo.CaballeroRosas@kaust.edu.sa), Angelica Coronado (Angelica.CoronadoPreciado@kaust.edu.sa) and Prof. Eric Feron (Eric.Feron@kaust.edu.sa) are with the Computer, Electrical and Mathematical Sciences and Engineering division, King Abdullah University of Science and Technology, Thuwal, Kingdom of Saudi Arabia. **Ph.D. students Renzo Caballero and Angelica Coronado contributed to this work equally.**

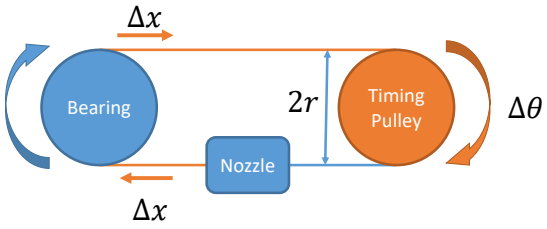

Fig. 1. Basic diagram of the pulley-belt system.

that the 3D printer utilizes by default. Thus, we define a non-ideal pulley as a pulley with any geometric shape or radius different from the ideal pulley.

In the case where the 3D printer has a non-ideal timing pulley on the x-axis, the relation between Δx and $\Delta\theta$ might not only depend on the angular rotation $\Delta\theta$, but also on the angular position of the pulley $\theta \in [0, 2\pi)$. Given a timing pulley C, we call the *instant displacement* of C to the function $f_C : [0, 2\pi) \to \mathbb{R}^+$ (with $\mathbb{R}^+$ denoting the non-negative real numbers) resulting from computing the limit (1) with the timing pulley C on the printer x-axis for all possible initial positions from 0 to 2π. Then, for a timing pulley C with initial angular position θ_0 and an angular displacement $\Delta\theta$, the relation between the x-axis nozzle displacement Δx and $\Delta\theta$ is given by

$$\Delta x = \int_{\theta_0}^{\theta_0+\Delta\theta} f_C(s)\,\mathrm{d}s. \tag{2}$$

The goal of the experiment is, for a non-ideal timing pulley C on the x-axis, to obtain the needed data to validate the computational evaluation from [15] of the instant displacement of C, f_C.

B. Experimental Steps

The utilized 3D printer in the experiment is an Ender-5 3D printer [28]—see Fig. 2-i)—. The 3D printer is composed of one stepper motor for material extrusion and three stepper motors that control the x, y, and z positions respectively. The x-axis and y-axis on the 3D printer use a belt-pulley transmission system for linear motion and positioning of the nozzle.

We utilize a room equipped with an Optitrack system composed of twenty Prime17w cameras with infrared LEDs for tracking. Opitrack tracks millimeter-scale movements with reliable precision using reflective markers.

Prior to the experiment, we design and 3D print six timing pulleys $\{C_1, C_2, \ldots, C_6\}$ (see Fig. 5) and two bases for the reflective markers (see Fig. 2-ii) and 2-iii)) with four attachment points each. One marker base is placed over the nozzle and the other on top of the timing pulley located on the x-axis motor, as shown in Fig. 2-i).

For each one of the six timing pulleys $\{C_1, C_2, \ldots, C_6\}$ with different shapes, we command the 3D printer to print lines parallel to the x-axis at three different printing speeds: $40\,\mathrm{mm\,s^{-1}}$, $80\,\mathrm{mm\,s^{-1}}$, and $120\,\mathrm{mm\,s^{-1}}$. We track the cartesian position over time of the markers placed on top of the nozzle, and we track the cartesian position and angular position over time of the marker placed on top of the timing pulley.

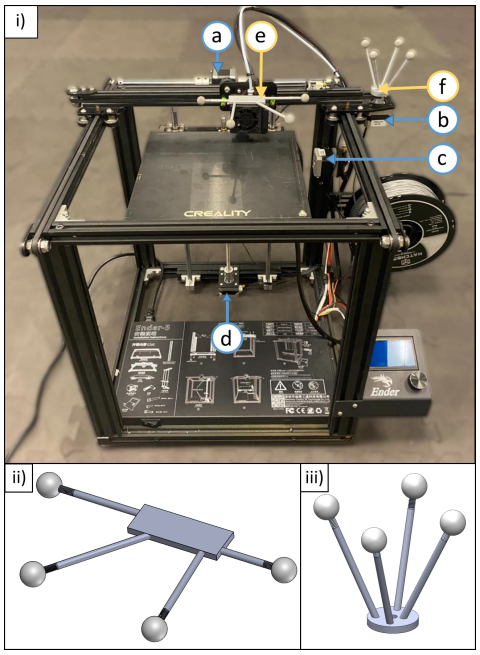

Fig. 2. Ender-5 3D Printer [28]: i)-a y-axis stepper motor, i)-b x-axis stepper motor, i)-c extruder stepper motor, i)-d z-axis stepper motor, i)-e nozzle marker base, and i)-f x-axis timing pulley marker base. CAD design: ii) nozzle marker base, and iii) x-axis timing pulley marker base.

A timing pulley identical to the ideal one, C_1, is utilized as one of the six subjects. The experiment with the ideal circular pulley C_1 provides the reference values to be utilized in the normalization of the other timing pulleys $\{C_2, \ldots, C_6\}$.

The raw data from the experiments, the CAD designs of the non-ideal pulleys, and the CAD design of the marker bases can be found on GitHub [29]. The recorded data is then processed and smoothed in MATLAB using the function $smoothdata$. Finally, the location of the nozzle is calculated with respect to the position where the nozzle starts the displacement parallel to the x-axis. A summary of the steps taken during the experiment can be seen in Fig. 3.

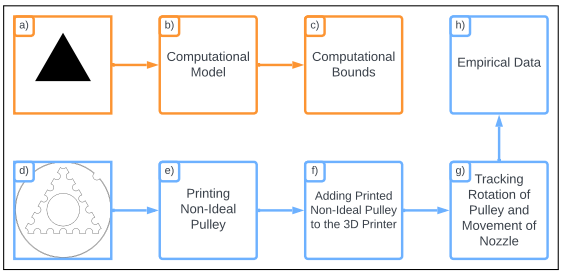

Fig. 3. Block representation of the steps taken during the simulation (a,b,c) and the experiment (d,e,f,g,h). Simulation blocks: a) two-dimensional design of a timing pulley C, b) simulation of the instant displacement f_C of the timing pulley C, c) simulation of bounds f_{H_I} and f_{H_O}, which depend on the misalignment between the pulley and belt teeth. Experiment blocks: d) CAD design of non-ideal timing pulley, e) printing of non-ideal timing pulley, f) replacing non-ideal pulley on the printer x-axis, g) performing tracking of the non-ideal pulley and nozzle dynamics, h) storing and smoothing experimental data.

III. Observations

Fig. 4 shows pictures of the timing pulley with an oval shape C_3 on the printer x-axis for the angular positions $\{0, \pi/2, \pi, 3\pi/2\}$. We observe a misalignment between the teeth of the belt and the teeth of the pulley in b), c), and d). Such misalignment occurs for all pulleys, except the ideal one C_1.

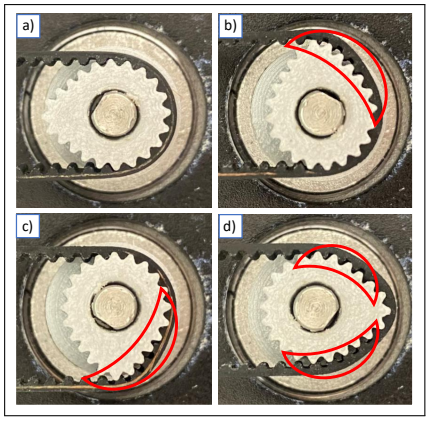

Fig. 4. Photo sequence of a 2π rotation (clockwise direction) of the oval pulley. The red outline marks the misalignment of the timing belt teeth with the teeth of the pulley.

Fig. 5 shows an example of normalized experimental instant displacement for each one of the six timing pulleys evaluated during the experiment. Each experimental instant displacement is calculated as the finite differences with respect to the timing pulley angular position of the vector position of the nozzle. The normalization value is calculated as the mean experimental instant displacement of the ideal timing pulley C_1. We observe oscillations within the interval $[0, 2\pi)$ depending on the number of symmetry angles on the timing pulley, e.g., the triangular pulley presents oscillations with period $2\pi/3$, and the squared pulley with period $\pi/2$.

A total of 108 rotations are recorded for each timing pulley. No significant differences are observed in the experimental data from different printing speeds, and all experimental data on the paper corresponds to a printing speed of $40\,\mathrm{mm\,s^{-1}}$.

IV. Computational Model

We present an extension of the model from [15] where teeth misalignment is considered. The extended model is validated with the experimental data. Also, we present a new mathematical model that characterizes the dynamics of the 3D printer nozzle, followed by a generalization that can be utilized in systems with multiple non-ideal timing pulleys, and where slippage and non-ideal tensions are considered. The system is assumed to be quasistatic, and no inertia is considered. We utilize our previous work [15] as a building block in the subsequent models.

A. Our Previous Work

In [15] we constructed a computational model that utilizes convex hull theory, calculus, and geometry to predict the influence of non-ideal timing pulleys on the printing process (Git repository: [30]). A timing pulley C is a three-dimensional ($C \subset \mathbb{R}^3$) body with two parallel identical faces (base and top) that are connected by a surface. In our model, we consider the two-dimensional cut parallel to the pulley base, and after we consider the convex hull of that two-dimensional figure, which we call $H \subset \mathbb{R}^2$ (see Fig. 6-left).

The modeling process in [15] is as follows: We consider a convex cover $H' \subset \mathbb{R}^2$ with a finite number of edges that covers the timing pulley convex hull, i.e., $H \subset H'$. Then, we discretize the convex cover into a discrete number of triangles where all of them share a common point, the center of rotation of the timing pulley, and by utilizing geometry, we find an exact expression for the instant displacement $f_{H'}$ of the pulley represented by the convex cover H'. Fig. 6-right shows an example of a timing pulley with a heart shape, where we can also see its discretized convex hull. Finally, an assumption in [15] is that both pulleys with the same convex hull have the same instant displacement, so we can assume $f_C = f_H$, and since H' can approximate H as much as needed, $f_{H'}$ approximates f_C as much as needed, begin the only limiting factor the resolution of H' in the simulation.

1) Teeth Misalignment in Computational Model: We consider two different convex sets in the model, where one set includes ($\subset$) the other set. The inner convex hull $H_I \subset \mathbb{R}^2$ corresponds to the convex hull of the timing pulley C when the teeth of the pulley and the teeth of the belt match perfectly (i.e., the ideal condition for such a system, or in other words, $H_I = H$). The outer convex hull $H_O \subset \mathbb{R}^2$ is constructed by assuming a complete misalignment between the teeth, by adding an offset to the contour of H_I. The relation between the two convex sets is $H_I \subset H_O$.

B. System with One Timing Pulley: 3D Printer

We model the dynamics of the printer with a non-ideal timing pulley following the notation and structure presented in Fig. 7, and utilizing the following:

Assumption 1: The timing belt does not stretch appreciably, i.e., its total length does not change.

This assumption is supported by the observations in Section III, where different stepper motor speeds affected the displacement of the nozzle equally. In addition, timing belts are designed to have minimal stretch [31].

Assumption 2: The timing belt is being pulled from exactly one point on the convex hull of the timing pulley.

Fig. 7 shows a graphical representation of the system we are analyzing. Points P_2 and P_3 are the top pulley-belt contact point and bottom pulley-belt contact point, respectively. When there is no slippage and the timing pulley has clockwise positive angular velocity, point P_2 pulls from the timing belt, causing the bearing to have a instant tangent velocity v_1. Point P_1 defines the location of the nozzle and is driven by the rest of the system.

1) Mathematical Formulation of the Belt States: For the i-th segment of the belt, with $i \in \{1, 2, 3\}$, or the segment delimited by the timing pulley (segment from P_2 to P_3), we define for all $t \in [t_0, t_1]$ the length with ideal tension

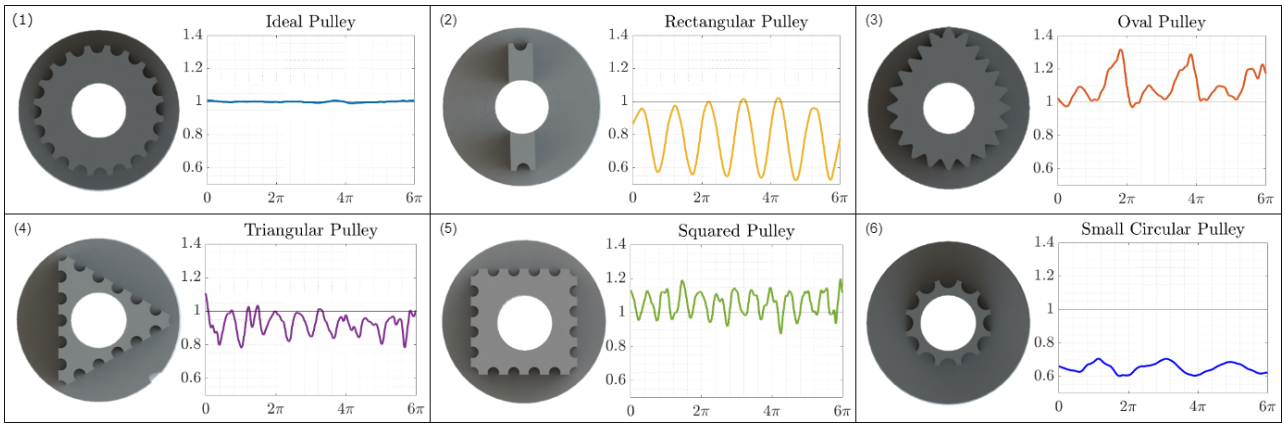

Fig. 5. Plot of experimental instant displacements for six different pulley geometries: (1) ideal circle-shaped pulley, (2) rectangular-shaped pulley, (3) oval-shaped pulley, (4) triangular-shaped pulley, (5) squared-shaped pulley, (6) small circle-shaped pulley.

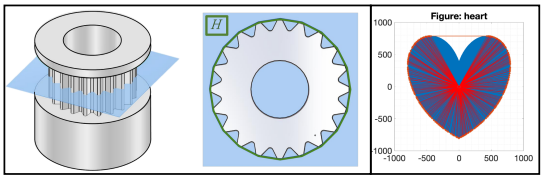

Fig. 6. Left: 3D model of an ideal pulley with a transverse cut parallel to the xy-plane. Right: example of a heart-shaped timing pulley included in a discrete convex hull.

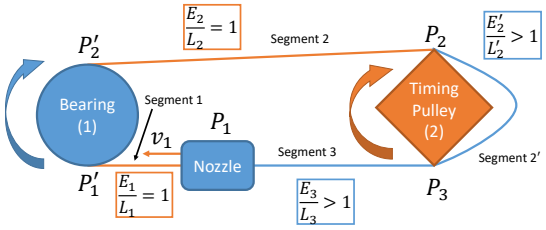

Fig. 7. Graphical representation of a system with a non-circular timing pulley, a timing belt, and a bearing.

$L_i(t) > 0$ and the actual length of the segment $E_i(t) > 0$, such that the total length $E > 0$ is time-invariant and given by $\sum_{i=1}^{3} E_i(t) + E_2'(t) = E$. Since the belt is not stretchable, there are only two possible states of tension: either ideal tension or loose. For each segment—including the one delimited by P_2 and P_3—, at time t, the states ideal or loose are given by:

$$\begin{cases} \frac{E_i(t)}{L_i(t)} > 1 \text{ loose timing belt,} \\ \frac{E_i(t)}{L_i(t)} = 1 \text{ timing belt with ideal tension.} \end{cases} \tag{3}$$

When the timing pulley starts rotating clockwise at time t_0, and the transition time from t_0 until t^* where $E_2(t) > L_2(t)$ ($t \in [t_0, t_*)$) has passed, the tension on the top line reaches its ideal value and then $E_2(t) = L_2(t)$ for $t \in [t^*, t_1]$.

The dynamics of the ideal tension $\{L_i(t)\}_{i=1}^{3}$ and $L_2'(t)$ are:

$$\begin{cases} L_1(t) = ||P_1' - P_1(t)||_2, \\ L_2(t) = ||P_2(t) - P_2'(t)||_2, \\ L_2'(t) = \text{Perimeter from } P_2 \text{ to } P_3 \text{ (clockwise)}, \\ L_3(t) = ||P_1(t) - P_3(t)||_2, \end{cases} \tag{4}$$

where we assume that the contact points with the bearing P_1' and P_2' have fixed positions, $P_2(t)$ and $P_3(t)$ are given by the control on the stepper motor, and $P_1(t)$ adapts such that Assumption 1 holds. Note that $\dot{L}_1(t) = -|v_1(t)|$, where $v_1(t)$ is the velocity of $P_1(t)$ at time t, which is aligned with wit the vector $P_1' - P_1(t)$. All of these functions and conditions are illustrated in Fig. 7.

C. System with Multiple Non-Ideal Timing Pulleys

We generalize the 3D printer x-axis pulley-nozzle dynamics to a system with a mobile mass, $n \in \mathbb{N}$ non-ideal timing pulleys rotating in a clockwise direction, $n+1$ ideal passive bearings with radius r, and a single timing belt, as shown in Fig. 8. The present model is at the risk of overfitting due to a large number of control variables (the controls for the timing pulleys). To guarantee a single solution, the possibility of slippage of the timing belt over the timing pulleys is considered and modeled.

Consider the $2n+2$ ideal lengths $\{L_i(t)\}_{i=1}^{2n+2}$ and actual lengths $\{E_i(t)\}_{i=1}^{2n+2}$ of the segments between the bearings and the pulleys. At time t, the $2i$-th timing pulley is pulling from the $(2i-1)$-th bearing when the $2i$-th segment has ideal tension, i.e., $E_{2i}(t)/L_{2i}(t) = 1$. We assume the contact points over the bearings $\{P_i'\}_{i=1}^{2n+2}$ to have a fixed location given by the distribution of the bearings, timing pulleys, and the mass in the system. The contact points over the timing pulleys $\{P_i(t)\}_{i=2}^{2n+1}$ are time-dependent and their location is given by the angular positions of each timing pulley in such a way that $L_i(t) = ||P_i(t) - P_i'||_2$. For the $2i$-th timing pulley, with $i \in \{1, \dots, n\}$, we consider the perimeter of its convex hull between points $P_{2i}(t)$ and $P_{2i+1}(t)$ (in the clockwise direction) as $L_{2i}'(t)$ and the portion of belt between the same

points as $E'_{2i}(t)$, where $E'_{2i}(t)/L'_{2i}(t) \geq 1$ (see Fig. 7 for an example where $E'_2/L'_2 > 1$).

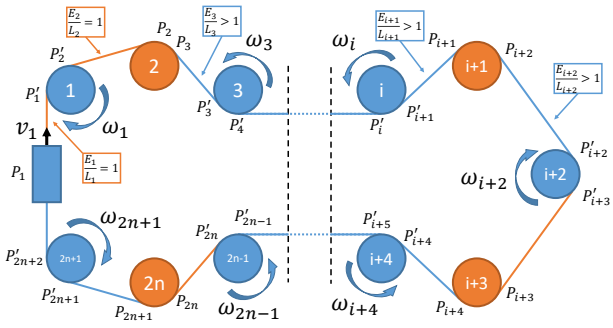

Fig. 8. Representation of an arbitrary system with $n \in \mathbb{N}$ non-ideal timing pulleys (orange), $n+1$ passive bearings (blue), and a mass. We neglect the segments of belt in contact with the bearings.

Observe the $(i+1)$-th timing pulley in Fig. 8. If we assume it rotates clockwise, and that its convex hull has a discrete number of vertices—needed assumption to utilize the model described in Subsection IV-A—, then, in a finite time interval $[t_0, t_1]$, there exist a set of n_{i+1} transition times $\{t_j^{(i+1)}\}_{j=1}^{n_{(i+1)}}$ such that $L_{i+1}(t_j^{(i+1)-}) > L_{i+1}(t_j^{(i+1)+})$, and they represent the exact time when the contact point belt-pulley changes, and $L_{i+1}(t)$ experiences a discrete change $\Delta L_j^{(i+1)} = L_{i+1}(t_j^{(i+1)-}) - L_{i+1}(t_j^{(i+1)+})$. We denote

$$J_{(i+1)}(t) = \sum_{j=1}^{n_{(i+1)}} \delta_{t_j^{(i+1)}}(t) \Delta L_j^{(i+1)}, \tag{5}$$

to the function describing the discrete jumps of $L_{(i+1)}(t)$ in $[t_0, t_1]$, where $\delta_x(t)$ denotes the Dirac delta with weight at $t = x$.

With the previous setup defined, we consider the conservation of mass for the non-flexible timing belt of length $E > 0$ for all time $t \in [t_0, t_1]$ as

$$E = \sum_{i=1}^{2n+2} E_i(t) + \sum_{i=1}^{n} E'_{2i}(t), \tag{6}$$

where we neglect the segments of belt in contact with the bearings, and for each individual segment:

$$E_{i+1}(t) = E_{i+1}(t_0) + \int_{t_0}^{t} \omega_i(s) r - J_{(i+1)}(s) - v^*_{i+1}(s)\, \mathrm{d}s, \tag{7}$$

$$E'_{i+1}(t) = E'_{i+1}(t_0) + \int_{t_0}^{t} v^*_{i+1}(s) + J_{(i+1)}(s) - J_{(i+2)}(s) - v^*_{i+2}(s)\, \mathrm{d}s, \tag{8}$$

and

$$E_{i+2}(t) = E_{i+2}(t_0) + \int_{t_0}^{t} J_{(i+2)}(s) + v^*_{i+2}(s) - \omega_{i+2}(s) r\, \mathrm{d}s, \tag{9}$$

where the set of velocities $\{v_i(t)\}_{i=2}^{2n+1}$ such that $\dot{L}_i(t) = (-1)^i |v_i(t)|$ almost everywhere in $t \in [t_0, t_1]$ is given by the control over the timing pulleys and modeled by the computational model in Subsection IV-A. Velocities $\{v_i^*\}_{i=2}^{2n+1}$ represent the slippage over the timing pulleys and are determined by the conservation of mass. For example, in Fig. 8, if we only consider the system composed of the $(i+1)$-th and $(i+3)$-th timing pulleys and the $(i+2)$-th bearing, and we assume that $\exists t^* \in [t_0, t_1]$ such that $\frac{E_{i+2}(t^*)}{L_{i+2}(t^*)} = \frac{E_{i+3}(t^*)}{L_{i+3}(t^*)} = 1$, and $v_{i+3}(t^*) > v_{i+2}(t^*)$, then $v^*_{i+2}(t^*) = v_{i+3}(t^*) - v_{i+2}(t^*)$. Finally, if we compute the derivative of (6), we observe that the total length does not change over time.

Thus, in a system constrained by the angular position of the timing pulleys, the location of the mass can be either fully determined (if we assume perfect matching of the teeth of the timing pulley and the timing belt) or partially determined within some confidence band if we assume misalignment for some pulleys.

V. Simulation and Validation

We validate the model with a single non-ideal timing pulley described in Subsection IV-B considering the misalignment described in Subsection IV-A.1, and we simulate a system with two non-ideal timing pulleys.

A. Validation of the Experimental Data

We verify our computational simulations from [15] with the teeth misalignment consideration described in Subsection IV-A.1 against the experimental data generated from the experiment described in Section II. The experiment represents a system with a single mass (nozzle), bearing, and a non-ideal timing pulley.

Fig. 3 shows the steps taken during the simulation and the experiment. The experiment starts with the CAD design of a non-ideal timing pulley, which is 3D printed, and then inserted into the 3D printer x-axis. In parallel, an equivalent two-dimensional pulley is drawn and inserted into the simulation. Finally, we compare the output of the computational and experimental systems. During the steps described in Fig. 3, the two initial conditions for the simulation and the experiment, a) and d), respectively, are constructed to agree on the dimensions.

Fig. 9 shows three experimental instant displacements starting from the same angular position and the simulated bounds for each of the six tested timing pulleys $(C_1, \ldots, C_6)$. The lower bound corresponds to the simulation of the instant displacements $\{f_{H_{I_1}}, \ldots, f_{H_{I_6}}\}$ assuming ideal teeth alignment, and the upper bound corresponds to the simulation of the instant displacements $\{f_{H_{O_1}}, \ldots, f_{H_{O_6}}\}$ assuming complete teeth misalignment. Notice that the experimental data fit into the bounds in most cases, whereas the other cases can be justified by data smoothing.

B. Simulation of a Multiple Pulley System

Fig. 10 shows the simulated system, where the timing pulleys 2 and 4 have squared and oval shapes, respectively.

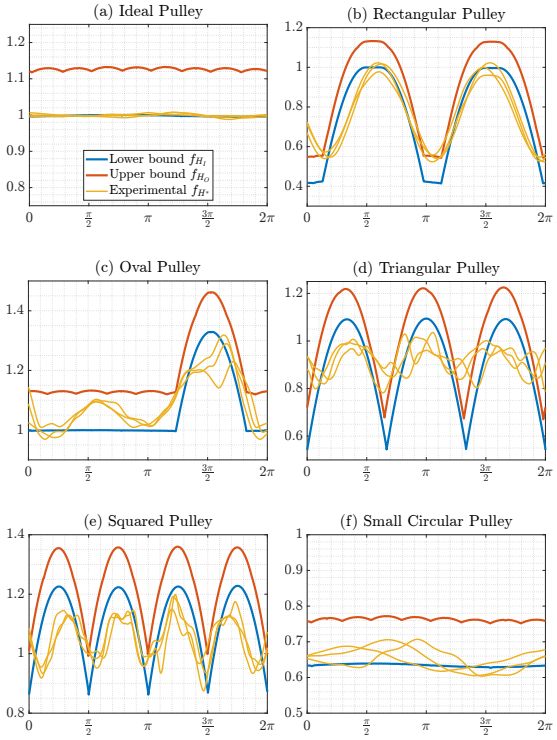

Fig. 9. Experimental instant displacement and simulated upper and lower bound in cases: (a) Ideal-shape pulley, (b) Rectangular-shape pulley, (c) Oval-shape pulley, (d) Triangular-shape pulley, (e) Squared-shape pulley, (f) Small circular-shape pulley. Each plot shows three experimental measurements starting from the same angular position.

The distance between the center of rotation between consecutive pulleys and bearings (bodies 1,2,3,4 and 5) is 100 mm. We simulate 10 seconds ($t_0 = 0\,\mathrm{s}$ and $t_1 = 10\,\mathrm{s}$) of operation where the angular velocities of pulleys 2 and 4 are $2\pi/5\ \mathrm{rad\,s^{-1}}$ and $4\pi/5\ \mathrm{rad\,s^{-1}}$, respectively. Pulley 4 is faster to ensure slippery over pulley 2. For this simulation, we are assuming perfect pulley-belt contact, and an initial slack factor of 10% for all lines, except for the second one, with a factor of 40%, i.e., $E_i(t_0)/L_i(t_0) = 1.1$ for $i \in \{1, 3, 4, 5\}$, and $E_2(t_0)/L_2(t_0) = 1.4$.

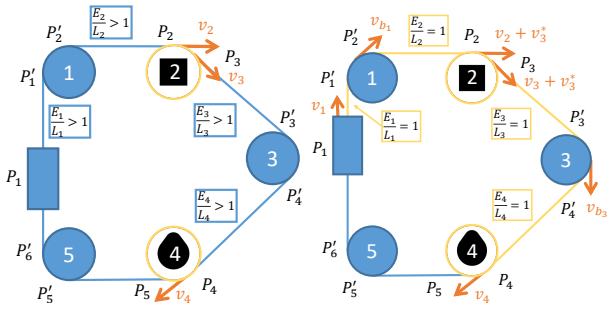

Fig. 10. Initial (left) and final (right) states condition of the system at times $t = t_0 = 0$ and $t = t_1 = 10$, respectively.

Under the previous conditions, the position of the mass is fully determined by the angular velocity of the timing pulleys. The exact position of the contact points over the timing pulleys, and the value of L_i over time with $i \in \{2, 3, 4, 5\}$ is given by the angular position of each timing pulley.

In Fig. 11 we observe the results from the simulation, where we can see the values over time of (a) $L_1(t)$ and $E_1(t)$, (b) $L_2(t)$ and $E_2(t)$, (c) $L_3(t)$ and $E_3(t)$, (d) $L_4(t)$ and $E_4(t)$, (e) position of the mass relative to its initial position, and (f) the velocities of the elements on the system. We can observe the discrete jumps described by (5) in plots (b), (c), and (d).

Notice that the mass is at rest until the time t^* such that $E_1(t)/L_1(t) = 1$ for $t \in [t^*, t_1]$. Also, observe that the system has slippery over the timing pulley 2 after t^{**} such that $E_3(t)/L_3(t) = E_4(t)/L_4(t) = 1$ for $t \in [t^{**}, t_1]$. All code regarding this simulation can be found in [29].

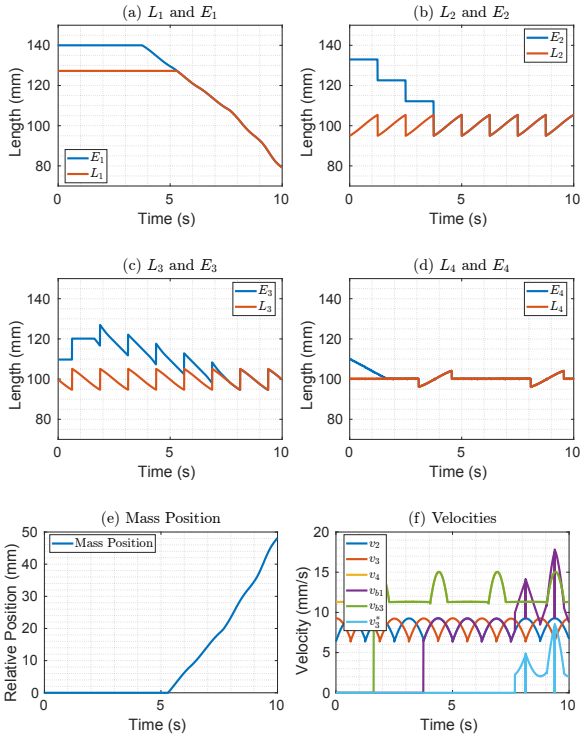

Fig. 11. Dynamics of the simulated system: (a) L_1 and E_1, (b) L_2 and E_2, (c) L_3 and E_3, (d) L_4 and E_4, (e) position of the mass relative to its initial position, (f) velocities of the elements on the system.

VI. Conclusion

This paper presents a computational model that successfully predicts the dynamics of a transmission system of a 3D printer with a non-ideal timing pulley on the printer x-axis. A total of six timing pulleys with different geometric shapes are tested at different printing speeds to collect the needed data to validate the model. We consider cases where the teeth of the timing pulley and the timing belt align perfectly, as well as those where there is a complete misalignment, to establish bounds for instant displacement. The model is extended to a case with multiple non-ideal timing pulleys and bearings where the slippage and non-ideal tension on the timing belt are considered. A simulation of a transmission system with two non-circular timing pulleys is presented and explained.

REFERENCES

[1] K. Yoshida and W. Khalil, "A New Model for Dynamic Behaviour of Timing Belt Drive Systems," *IFAC Proceedings Volumes*, vol. 33, no. 26, pp. 631–636, 2000, iFAC Conference on Mechatronic Systems, Darmstadt, Germany, 18-20 September 2000. [Online]. Available: https://www.sciencedirect.com/science/article/pii/S1474667017392169

[2] M. Ashkvari, A. Yousefi-Koma, H. Keshavarz, and M. Shariat-Panahi, "Design improvement of a 2-DOF ankle joint actuation mechanism for a humanoid robot," in *2016 4th International Conference on Robotics and Mechatronics (ICROM)*, 2016, pp. 439–444.

[3] M. Khazaee, A. Banakar, B. Ghobadian, M. A. Mirsalim, and S. Minaei, "Remaining useful life (RUL) prediction of internal combustion engine timing belt based on vibration signals and artificial neural network," *Neural Computing and Applications*, vol. 33, no. 13, pp. 7785–7801, 2021.

[4] M. Ucar, R. Ergun, and A. Cengiz, "A novel failure diagnosis system design for automotive timing belts," *Experimental Techniques*, vol. 38, no. 5, pp. 48–53, 2014.

[5] A. R. Hassan and K. M. Ali, "Dignosis of pulley-belt system faults using vibration analysis technique," *Journal of University of Babylon for Engineering Sciences*, vol. 26, no. 2, pp. 167–180, 2018.

[6] Y. Lo, T. Yeh, and Y.-C. Shu, "SECE-based piezoelectric energy sensor for the diagnostics of timing belt," in *Active and Passive Smart Structures and Integrated Systems XVI*, vol. 12043. SPIE, 2022, pp. 273–281.

[7] B. STOJANOVIca, N. MILORADOVIca, N. MARJANOVIca, M. BLAGOJEVIca, and A. MARINKOVIcb, "Wear of Timing Belt Drives," *Journal of the Balkan Tribological Association Vol*, vol. 17, no. 2, pp. 206–214, 2011.

[8] R. Perneder and I. Osborne, "Timing Belt Failure," in *Handbook Timing Belts*. Springer, 2011, pp. 243–249.

[9] S. Passos, L. Manin, D. Remond, O. Sauvage, L. Rota, and E. Besnier, "Investigation on the rotational dynamics of a timing belt drive including an oval driving pulley," *Journal of Vibration and Acoustics*, vol. 143, no. 5, 2021.

[10] J.-w. Suh and K.-y. Kim, "Harmonious cable actuation mechanism for soft robot joints using a pair of noncircular pulleys," *Journal of Mechanisms and Robotics*, vol. 10, no. 6, p. 061002, 2018.

[11] P. Krawiec, D. Czarnecka-Komorowska, Ł. Warguła, and S. Wojciechowski, "Geometric Specification of Non-Circular Pulleys Made with Various Additive Manufacturing Techniques," *Materials*, vol. 14, no. 7, p. 1682, 2021.

[12] G. Endo, H. Yamada, A. Yajima, M. Ogata, and S. Hirose, "A weight compensation mechanism with a non-circular pulley and a spring: Application to a parallel four-bar linkage arm," *SICE Journal of Control, Measurement, and System Integration*, vol. 3, no. 2, pp. 130–136, 2010.

[13] D. Ludovico, P. Guardiani, F. Lasagni, J. Lee, F. Cannella, and D. G. Caldwell, "Design of Non-Circular Pulleys for Torque Generation: A Convex Optimisation Approach," *IEEE Robotics and Automation Letters*, vol. 6, no. 2, pp. 958–965, 2021.

[14] Y. Tsuneoka and I. Mizuuchi, "Design method of non-circular pulleys for pneumatic-driven musculoskeletal robots that generate specific direction force by one-shot valve operations," in *2015 IEEE International Conference on Robotics and Biomimetics (ROBIO)*. IEEE, 2015, pp. 553–558.

[15] R. Caballero and E. Feron, "Experiments in Robotic Self-Repair: A 3D Printer Repairs Its Own Timing Pulley," in *2022 American Control Conference (ACC)*, 2022, pp. 3702–3709.

[16] Caballero, Renzo and Feron, Eric, "Study of Fixed-Points in the Self-Repair Process of a 3D Printer," *IEEE Control Systems Letters*, 2022.

[17] D. A. Maravi R, G. M. Iparraguirre O, and S. R. Prado G, "Implementation of a Digital PID Control for the Compensation of Loss Steps from CORE XY 3D Printer Motors Working at High Speeds," in *2020 IEEE ANDESCON*, 2020, pp. 1–6.

[18] A. Munteanu, D.-F. Chitariu, M. Horodinca, C.-G. Dumitras, F. Negoescu, A. Savin, and F. Chifan, "A Study on the Errors of 2D Circular Trajectories Generated on a 3D Printer," *Applied Sciences*, vol. 11, no. 24, p. 11695, 2021.

[19] S. Mihcin, H. Kose, S. Cizmeciogullari, S. Ciklacandir, M. Kocak, A. Tosun, and A. Akan, "Investigation of Wearable Motion Capture System Towards Biomechanical Modelling," in *2019 IEEE International Symposium on Medical Measurements and Applications (MeMeA)*, 2019, pp. 1–5.

[20] Z. Wu and L. Zheng, "Emotional Communication Robot Based on 3D Face Model and ASR Technology," in *2019 IEEE 9th International Conference on Electronics Information and Emergency Communication (ICEIEC)*, 2019, pp. 1–4.

[21] A. Mori and Y. Itoh, "DroneCamo: Modifying Human-Drone Comfort via Augmented Reality," in *2019 IEEE International Symposium on Mixed and Augmented Reality Adjunct (ISMAR-Adjunct)*, 2019, pp. 167–168.

[22] J. Song, Z. Liu, X. Liu, and J. Guo, "Tightly coupled Visual Inertial Odometry based on Artificial Landmarks," in *2018 IEEE International Conference on Information and Automation (ICIA)*, 2018, pp. 63–70.

[23] W. Ye, Z. Li, C. Yang, J. Sun, C.-Y. Su, and R. Lu, "Vision-Based Human Tracking Control of a Wheeled Inverted Pendulum Robot," *IEEE Transactions on Cybernetics*, vol. 46, no. 11, pp. 2423–2434, 2016.

[24] F. C. Can, M. Hepeyiler, and Ö. Başer, "A novel inverse kinematic approach for delta parallel robot," *International Journal of Materials, Mechanics and Manufacturing*, vol. 6, no. 5, pp. 321–326, 2018.

[25] J. Sustarevas, D. Kanoulas, and S. Julier, "Autonomous Mobile 3D Printing of Large-Scale Trajectories." IEEE, 2022.

[26] M. Vélez, E. Toala, and J. C. Zagal, "Koala 3D: A continuous climbing 3D printer," *Robotics and Computer-Integrated Manufacturing*, vol. 64, p. 101950, 2020.

[27] J. Sustarevas, K. X. Benjamin Tan, D. Gerber, R. Stuart-Smith, and V. M. Pawar, "YouWasps: Towards Autonomous Multi-Robot Mobile Deposition for Construction," in *2019 IEEE/RSJ International Conference on Intelligent Robots and Systems (IROS)*, 2019, pp. 2320–2327.

[28] "Creality Ender 5 Pro CAD Model," https://grabcad.com/library/creality-ender-5-pro-1, accessed: 2021-08-22.

[29] "System with Non-Ideal Timing Pulleys." [Online]. Available: https://github.com/RenzoCab/Non-Circular-Pulleys

[30] "Experiment in robotic self-repair: Git Repository." [Online]. Available: https://github.com/RenzoCab/Simulation-Gear-Belt

[31] R. G. Budynas, J. K. Nisbett *et al.*, *Shigley's Mechanical Engineering Design*. McGraw-hill New York, 2011, vol. 9.